Seventh International Conference on CFD in the Minerals and Process Industries
CSIRO, Melbourne, Australia
9-11 December 2009

CFD SIMULATION OF GAS-LIQUID FLOW IN A LARGE SCALE FLOTATION CELL

T. SONG, J. W. ZHOU, Z. C. SHEN

Beijing General Research Institute of Mining and Metallurgy, 1 Wenxing St., Xizhimenwai, Beijing 100044, China

ABSTRACT

The actual performance of a new flotation cell must be examined through the industrial tests. Since the situations of the industrial tests are different from the laboratory tests, people cannot know the hydrodynamic features in the flotation cells and it is hard to examine in the industrial test situations. CFD simulation of flotation cells provides a tool to get the hydrodynamic features and to analyse the influence of variations in design features and operating conditions on the performance of flotation cells. A large scale flotation cell designed by BGRIMM has been modelled. Complex gas-liquid flow fields within the cells and the gas volume fraction are predicted. The surface velocity of gas and the power requirement at varying impeller speeds and gas flow rates have been found to compare against measured values obtained from the industrial tests. The effects of some boundary conditions, such as the outlet setting and the timescale which are important to the model, have been discussed. The effects of impeller speed and gas flow rate on the flow fields in the large scale flotation cell have been investigated using computational modelling.

NOMENCLATURE

A added mass force [N m^{-3}]
C viscosity coefficient [dimensionless]
F drag force [N m^{-3}]
$\mathbf{g}$ gravity vector [m s^{-2}]
k turbulent kinetic energy [m^2 s^{-2}]
L lift force [N m^{-3}]
p pressure [Pa]
r volume fraction[dimensionless]
S source
t time[s]
T turbulent dispersion force [N m^{-3}]
$\mathbf{U}$ velocity vector [m s^{-1}]

Greek letters

ε turbulent eddy dissipation [s^{-1}]
ρ density [kg m^{-3}]
μ dynamic viscosity [N s m^{-2}]

Subscripts

L laminar
T turbulent
α phase number
β phase number

INTRODUCTION

Many Chinese ore bodies are in low grade, but 80% of Chinese plants are equipped with small flotation cells whose sizes are under 20 m^3 (Shen *et al.*, 2008). It is clear that using larger sized flotation cells can treat the low grade ore bodies economically and efficiently. Over the past ten years, Beijing General Institute of Mining and Metallurgy (BGRIMM) has focused on the research of large size flotation cells. Since 2000 the flotation cell sizes of KYF series, which are designed by BGRIMM, have steadily increased from 50 m^3 in 2000 to 320 m^3 in 2008. The largest flotation cell which has been used in plant has an effective capacity of 200 m^3. And the KYF-320 flotation cell whose size is 320 m^3 has been examined through the industrial tests in 2008. Figure 1 gives a picture of the development of BGRIMM large flotation cell sizes.

One important development area of the recent decade has been Computational Fluid Dynamics. This powerful tool can help to get quick estimation of new designs, cell hydrodynamics optimisation and process optimization by determining optimum setups for each process (Bourke , 2007). There have been lots of investigations on CFD model for flotation cells, and the key for reliable modelling method is the validation work in laboratory and industrial test. Since the size of the largest KYF flotation cell has been 320 m^3, whether the CFD model that has been validated in laboratory is suitable for this kind of big-size flotation cell is a problem we have to solve.

The work in this paper is to validate the CFD model of KYF-320 flotation cell by comparing some feature values between the prediction from CFD model and industrial test, and then amend the CFD model.

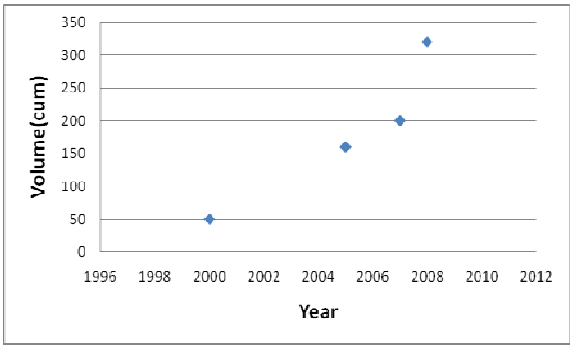

Figure 1: Historical development of BGRIMM large flotation cell sizes.

MODEL DESCRIPTION

Modelling of the gas-liquid flow has been carried out using an Eulerian two-fluid model, where the phases are treated as interpenetrating continua and conservation equations are solved for each phase (Koh and Schwarz *et al.*, 2003;Lane and Schwarz *et al.*, 2005). The continuity equations and momentum equations take the following form (where $\alpha = 1$ for liquid, $\alpha = 2$ for gas):

$$\frac{\partial(r_\alpha \rho_\alpha)}{\partial t} + \nabla \cdot (r_\alpha \rho_\alpha \mathbf{U}_\alpha) = S_{MS_\alpha} \quad (1)$$

$$\frac{\partial(r_\alpha \rho_\alpha \mathbf{U}_\alpha)}{\partial t} + \nabla \cdot [r_\alpha (\rho_\alpha \mathbf{U}_\alpha \otimes \mathbf{U}_\alpha)] = -r_\alpha \nabla p_\alpha + \nabla \cdot \left\{ r_\alpha \mu_\alpha \left[\nabla \mathbf{U}_\alpha + (\nabla \mathbf{U}_\alpha)^{\mathrm{T}} \right] \right\} + S_{M_\alpha} + M_\alpha + \sum_{\beta=1}^{N_p} \left(\Gamma^+_{\alpha\beta} \mathbf{U}_\beta + \Gamma^+_{\beta\alpha} \mathbf{U}_\alpha \right) + r_\alpha \rho_\alpha \mathbf{g} \quad (2)$$

Here r_α is the phase volume fraction, ρ_α is the density, t is time, and $\mathbf{U}_\alpha$ is the mean velocity vector. In the continuity equation, S_{MS_α} is a mass source term. In the momentum equation, S_{M_α} describes momentum sources due to external body forces and user defined momentum sources, M_α is the interfacial forces acting on phase α due to the presence of other phases, $\left(\Gamma^+_{\alpha\beta} \mathbf{U}_\beta - \Gamma^+_{\beta\alpha} \mathbf{U}_\alpha\right)$ represents momentum transfer induced by interphase mass transfer, and N_p is the total number of phases (here the value is 2).

By applying the eddy viscosity hypothesis, the Reynolds stresses can be linearly related to the mean velocity gradients in a manner analogous to the relationship between the stress and strain tensors in laminar Newtonian flow, so the effective turbulent stress tensor can be written in the $r_\alpha \mu_\alpha \left[\nabla \mathbf{U}_\alpha + (\nabla \mathbf{U}_\alpha)^{\mathrm{T}} \right]$ form.

The effective viscosity is sum of the laminar and turbulent viscosities:

$$\mu_\alpha = \mu_L + \mu_T \quad (3)$$

The turbulent viscosity in each phase is calculated using the standard $k - \varepsilon$ turbulence model:

$$\mu_T = C_\mu \rho \frac{k^2}{\varepsilon} \quad (4)$$

Turbulence kinetic energy k and turbulence dissipation rate ε are solved based on each phase velocity field.

The interfacial forces term is taken to be a sum of several forces, given by

$$M_\alpha = F_\alpha + A_\alpha + L_\alpha + T_\alpha \quad (5)$$

where F_α is the drag force, A_α is the added mass force, L_α is the lift force and T_α is the turbulent dispersion force. The interfacial forces are available as an option in the CFX 10.0 code (Ansys CFX-Solver, Release 10.0: Theory, 2005).

In the model, the impeller motion is treated by the multiple frames of reference method. The transport equations are solved using the CFD code CFX 10.0.

EXPERIMENTAL METHOD

The whole industrial tests are in a gas-water environment and the measurement values, including gas flow rate, gas dispersion rate, impeller speed, power consumption, gas volume fraction and the diameters of the bubbles, are obtained from the tests. Because of the big size of the flotation cell and the symmetry of the liquid surface, the test points are distributed in half of the round flat top, which represents an equal area of the surface, respectively. The positions of the test points are shown in the following picture (Figure 2, 32 points totally).

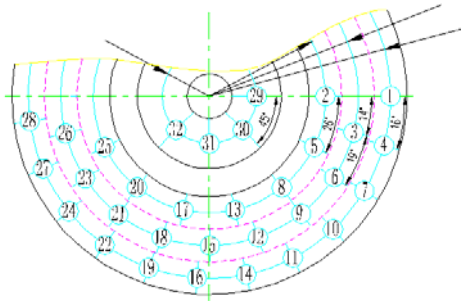

Figure 2: Positions of the gas flow rate measurement points in industrial tests.

The conditions of the industrial tests, including impeller speed and the original gas flow rate, are shown in the following table.

Case No.	1	2	3	4	5
D mm	327	342	357	372	387
V rpm	98	102	107	111	115

Table 1: The impeller speeds in different conditions (D represents the diameter of the actuating unit; V represents the impeller speed).

Case No.	1	2	3	4
R m^3/m^2min	1.0	1.1	1.2	1.3
A m^3/min	46.92	51.61	56.30	61.00

Table 2: The gas flow rates in different conditions (R represents the gas flow rate; A represents the amount of the gas consumption).

RESULTS AND DISCUSSION

The CFD mesh of the KYF-320 flotation cell has 84,825 nodes and 432,110 elements which are tetrahedral. To reduce the solution time, the mesh used is a little coarse. It was operated with an impeller speed of 107 rpm with the resulting fluid pressure on the KYF impeller and stator as indicated in Figure 3 and Figure 4. The high pressure areas' positions, which are red in the contour plots, have a good agreement with the industrial experience. The photos from the plant show that the upwind sides of the impeller blades and the top parts of the stator baffles have more abrasion than other areas.

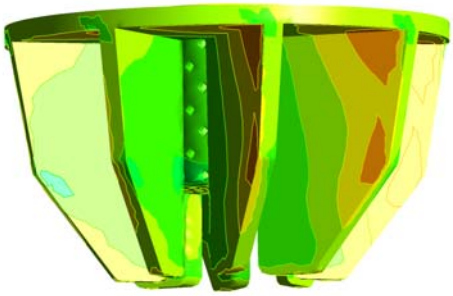

Figure 3: KYF impeller coloured by fluid pressure.

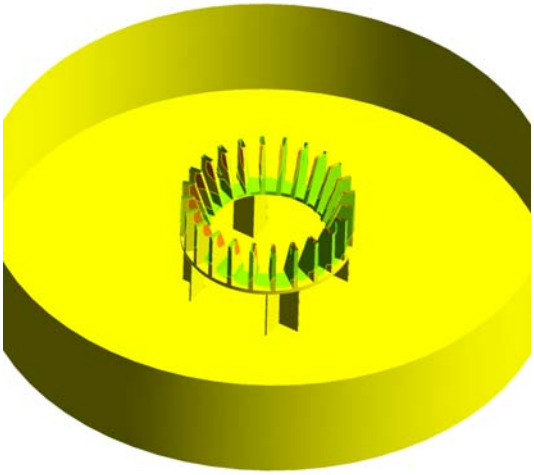

Figure 4: KYF stator coloured by fluid pressure.

The flow patterns of water and gas are shown in Figure 5 and Figure 6. The impeller generates a jet stream in the radial direction towards the wall, and the predicted flow pattern of water consists of two vortexes, with one vortex below the impeller and another above the impeller. The water flow circulates back to the impeller through the top and bottom of the stator. The gas flow basically circulates with the water flow but does not have conspicuous vortexes.

In the impeller region, there is a substantial region with high gas volume fraction 0.75-1.00 forming a cavity regime. Figure 7 shows that the gas moves in a circulatory motion within the cavity.

Comparisons are made of the measured and predicted gas velocity in the top of the flotation cell. As shown in Figure 8, the green points represent the predicted gas velocity and the black ones represent the measured values from the industrial tests. Since there is a groove on the top of the flotation cell, the predicted velocities in this area (from 1.5m to 2.0m in the radial direction) are much lower than the values got from other areas. The agreement is good between the measured and predicted velocities either in directions or in absolute values. The predicted power draw agrees well with the measured value too.

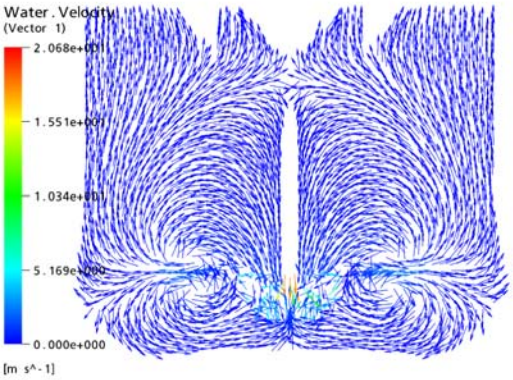

Figure 5: CFD predicted water velocity vectors in a vertical plane in the KYF-320 cell.

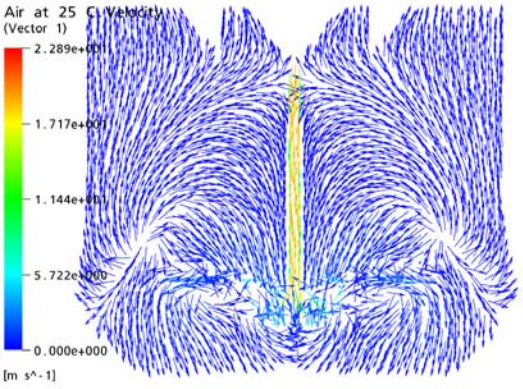

Figure 6: CFD predicted air velocity vectors in a vertical plane in the KYF-320 cell.

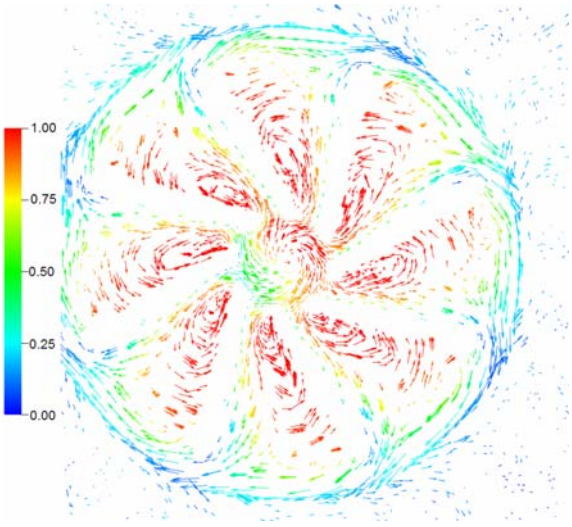

Figure 7: Predicted gas velocity vectors coloured by gas volume fraction illustrating cavity formation.

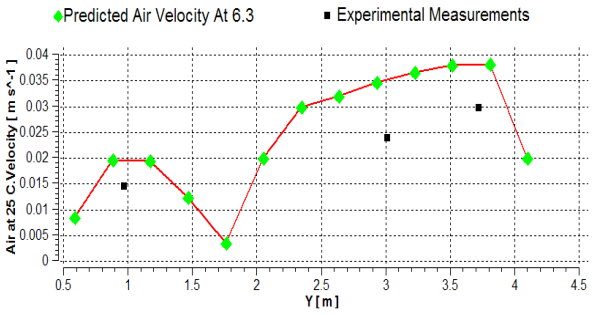

Figure 8: Predicted air velocity compared with experimental measurements.

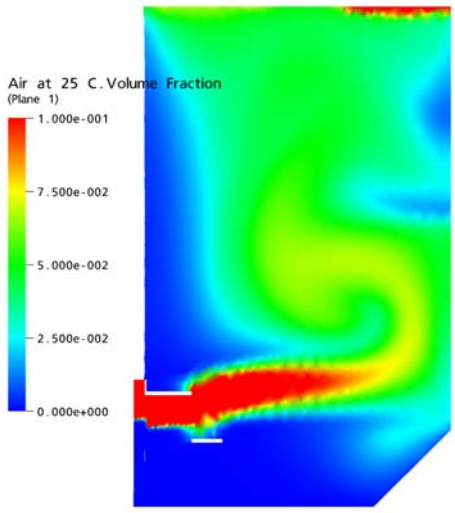

Figure 9: CFD predicted gas volume fraction in a vertical plane in the KYF-320 cell.

The predicted gas volume fraction in this model does not have an agreement with the measured value. The predicted value is less than 1%, but the measured values are from 11.14% to 12.88%, which are in different initial conditions. There have been some investigations on CFD models for flotation cells and stirred tanks which use the hexahedral elements that give good results in predicting the gas volume fraction in lab (Lane and Schwarz *et al.*, 2005; Koh and Schwarz, 2007). And the outlet boundary condition they use is pressure outlet condition or degassing condition. But the two outlet boundary conditions are not suitable for the model using tetrahedral elements, and there will be an error when a wall is placed at point(s) of an outlet boundary condition. This has been tested in CFX 10.0 environment.

Since the two outlet boundary conditions talked above do not work well, a new outlet boundary condition is used in the model. For reducing the calculation time, the new geometry is represented by a 90^o section containing just two impeller blades and 1/4 of the total stator baffles, with 68,729 nodes and 380,453 tetrahedral elements. At the liquid surface, the boundary condition is opening condition, and the initial gas volume fraction is 1. Figure 9 shows the predicted gas volume fraction in a vertical plane in the cell. The distribution of the gas volume fraction values in the figure has an agreement with the industrial experience and the experiment in lab. There is little gas in the bottom of the tank, and the gas volume fraction value is biggest in the mixing area. Through the volume integral, the gas volume fraction of the whole tank is 6.82%, which is between the value from the first model and the value from industrial test. In the meantime, the second model has a bigger gas velocity and does not have the "regular" flow pattern in the top of the tank.

Under the pressure outlet boundary condition and the degassing condition, the predicted flow pattern remains fairly similar when the impeller speed varies from 98 rpm to 115 rpm. Under the opening condition, the jet generated by the impeller will have a positive angle with the radial direction, and the angle will decrease when the impeller speed varies from 98 rpm to 115 rpm. And in this condition, the gas volume fraction will get bigger when turning the gas flow rate stronger.

CONCLUSION

The hydrodynamics in a large scale flotation cell fitted with KYF-320 flotation mechanism has been studied using CFD modelling. In the investigation, two kinds of outlet boundary conditions have been used to study the gas volume fraction. Modelling results under different initial conditions demonstrate good agreement with measurement values for gas velocity, fluid pressure, fluid pattern and power consumption. The gas volume fraction in the model using tetrahedral elements has been improved. In general, the modelling method is suitable for the large scale flotation cell, and the model can give good advices for investigations on the design and operation of flotation cells.

REFERENCES

P.T.L. KOH, M.P. SCHWARZ, Y. ZHU, P. BOURKE, R. PEAKER and J.P. FRANZIDIS, (2003), "Development of CFD models of mineral flotation cells", *Third International Conference on CFD in the Minerals and Process Industries*, Melbourne, Australia, December 10-12.

G.L. LANE, M.P. SCHWARZ and G.M. EVANS, (2005), "Numerical modelling of gas-liquid flow in stirred tanks", *Chemical Engineering Science*, 60, 2203-2214.

ANSYS CFX-Solver, Release 10.0: Theory, (2005), Computational Fluid Dynamics Services, ANSYS Canada Ltd., Waterloo, Ontario, Canada.

PETER BOURKE, (2007), "Optimising large flotation cell hydrodynamics using CFD", *Output Australia*, 19, 1-4.

P.T.L. KOH and M.P. SCHWARZ, (2007), "CFD model of a self-aerating flotation cell", *Int. J. Miner. Process*, 85, 16-24.

Z.C. SHEN, S.J. LU and L.J. YANG, (2008), "R&D and application of KYF large flotation cells developed by BGRIMM", *Nonferrous Metals*, 4, 115-119.

Z.C. SHEN, (2009), "Research and design of 200m^3 air forced flotation machine", *Nonferrous Metals*, 2, 100-103.